"Physics of Auroral Phenomena", Proc. XXXII Annual Seminar, Apatity, pp. 59 - 62, 2009

Polar Geophysical Institute

IONOSPHERIC CONVECTION FROM CLUSTER EDI MEASUREMENTS: COMPARISON WITH THE GROUND-BASED IZMEM IONOSPHERIC CONVECTION MODEL

M.Förster[1], Y.I.Feldstein[2], S.E. Haaland[3,4], L.A. Dremukhina[2], L.I. Gromova[2], A.E. Levitin[2]

[1]*Helmholtz-Zentrum Potsdam, GeoForschungsZentrum (GFZ), 14473 Potsdam, Germany*
[2]*IZMIRAN, Troitsk, Moscow region, Russia*
[3]*Max-Planck-Institut für Sonnensystemforschung, Lindau-Katlenburg, Germany*
[4]*Department of Physics and Technology, University of Bergen, Norway*

Abstract. Cluster/EDI electron drift observations above the Northern and Southern high-latitude areas for more than six and a half years (Feb 2001 till Oct 2007) have been used to derive a statistical model of the electric potential distribution for summer conditions. Based on potential pattern for different orientations of the interplanetary magnetic field (IMF) in the GSM *y-z* plane, basic convection pattern (BCP) were derived, that represent the main characteristics of the electric potential distribution in dependence on the IMF. The BCPs comprise the IMF-independent potential distribution as well as patterns, which describe the dependence on positive and negative IMF *Bz* and IMF *By* variations. The full set of BCPs compiles a Cluster model of ionospheric convection that allows to describe the spatial and temporal variation of the high-latitude electric potential (ionospheric convection) for any solar wind IMF conditions near the Earth`s magnetopause. The comparison of the Cluster/EDI model with the IZMEM ionospheric convection model, which was derived from ground-based magnetometer observations, shows a good agreement of the basic patterns and their variations with the IMF. According to the statistical model, there is a two-cell anti-sunward convection within the polar cap for northward IMF $Bz^+ \leq 2nT$, while for increasing northward IMF Bz^+ there appears a region of sunward convection within the high-latitude daytime sector, which assumes the form of two additional cells with sunward convection between them for IMF $Bz^+ \sim 4 \div 5nT$. This results in a four-cell convection pattern of the high-latitude convection. In dependence of the ±IMF *By* contribution during sufficiently strong northward IMF *Bz* conditions, a transformation to three-cell convection patterns appears.

Introduction

Models of high-latitude convection parameterized by Solar Wind parameters (plasma velocity, density and IMF components), are mainly based on measurements onboard of low-altitude satellites like, e.g.,OGO 6 [*Heppner*, 1977], DE 2 [*Heppner and Maynard*, 1987; *Weimer*, 1995, 2005] and DMSP [*Rich and Hairston*,1994 and *Papitashvili and Rich*, 2002] or ground-based observations with radar [*Ruohoniemi and Greenwald*, 2005, SuperDARN], or magnetometers networks [*Frees-Christensen et al*.,1985**;** *Feldstein and Levitin*, 1986].

In this paper we present a model of high-latitude convection based on measurements in the distant magnetosphere by the Electron Drift Instrument (EDI) of three CLUSTER satellites from February 2001 till October 2007. The Cluster/EDI model is compared with the IZMEM ionospheric convection model, which utilizes a linear regression between the IMF components and ground-based geomagnetic data of magnetometer stations at northern high latitudes. IMF-independent potential distribution and patterns described the dependence on positive and negative IMF *Bz* and *By* variations, are basic patterns to construct "elementary" current systems which cause the geomagnetic field variations. These current systems were used in *Feldstein and Levitin* [1986] to derive BCP.

The data

The method of data treatment and the procedure of IMF direction sorting is described in *Haaland et al.* [2007], *Förster et al.*[2007,2008]. EDI directly measures the full two- dimensional drift velocity (electric field), perpendicular to the magnetic field. The EDI measurements are mapped into the ionosphere to 400 km altitude using the Tsyganenko T2001 model [*Tsyganenko*, 2002]. The mapped vectors are then binned and averaged in bins with 2° width in latitude and a variable longitude width such that the bin area projected to the Earth`s surface is constant.

Due to orbit constraints, the local time coverage of the CLUSTER data in each hemisphere is tightly correlated with season; during the northern summer (June-August) the daytime-afternoon sector is covered, while during northern winter (December-February) it is the night-time to early morning sector. To obtain a statistical model of the high-latitude electric potential distribution (MLAT < 74º) for summer condition in the Northern hemisphere, we use data around northern summer solstice (March to September) and project Southern hemisphere observation of the half year around the southern summer solstice (September to March) into the Northern hemisphere with an inverted sign of IMF *By*.

Potential distributions

CLUSTER/EDI measurements of drift velocity or electric field were used to construct the ionospheric convection model. The usual way to represent high-latitude convection results is in terms of the electric potential distribution. High –latitude potential patterns were sorted for 8 different orientations (sectors) of IMF in the GSM *y-z*-plane. Each sector comprises 45°. Table 1 lists the average values of the IMF *By* and *Bz* components for all the data points that were used for the construction of each individual sector's potential patterns.

A spherical cap harmonic analysis [*Haines*, 1985] is applied for the high-latitude area with an equatorward boundary at colatitude 32°;the number of spherical harmonics is equal to 10.The expansion of the IZMEM model is described in в *Dremukhina et al.* [1998]. The analytical representation for each sector was obtained as synthesis of electric potentials in the grid points with spacing 1º in latitude and 1 hour in MLT.

Table 1. Averages of the IMF *By* and *Bz* component values at the magnetopause for all data used for the potential pattern of the respective sector.

Sector	IMF orientation	*By*	*Bz*
Sector 0	*Bz+*	0.00346	3.7207
Sector 1	*Bz+/By+*	3.3163	2.8274
Sector 2	*By+*	4.6262	-0.0495
Sector 3	*Bz-/By+*	3.3620	-2.8269
Sector 4	*Bz-*	-0.1406	-4.7503
Sector 5	*Bz-/By-*	-3.8990	-3.4105
Sector 6	*By-*	-5.0792	-0.0964
Sector 7	*Bz+/By-*	-3.5713	3.0543

Fig. 1 shows the potential patterns representing summer conditions of both hemispheres merged together. They are nearly identical to the patterns shown in *Haaland et al.* [2007, Fig.7] and *Förster et al.* [2008, Fig.1], which are based on data of the full year.

The following large-scale characteristics of the potential patterns in Fig. 1 can be noticed:

1) independent of the IMF orientation, always exists the familiar two-cell convection pattern with antisunward convection between the cells over the polar cap ;

2) for IMF *Bz < 0,* the two-cell antisunward convection pattern in the polar cap intensifies, which can be interpreted as an additional two-cell pattern with antisunward convection, overlayed on the similar pre-existing two-cell background pattern;

3) for IMF *Bz > 0,* there appears an additional pair of convection cells at high latitudes (> 80º) with sunward convection between them, which can be interpreted as an additional two-cell structure within the dayside polar cap, overlayed on the larger two-cell background and resulting in an overall four-cell convection pattern;

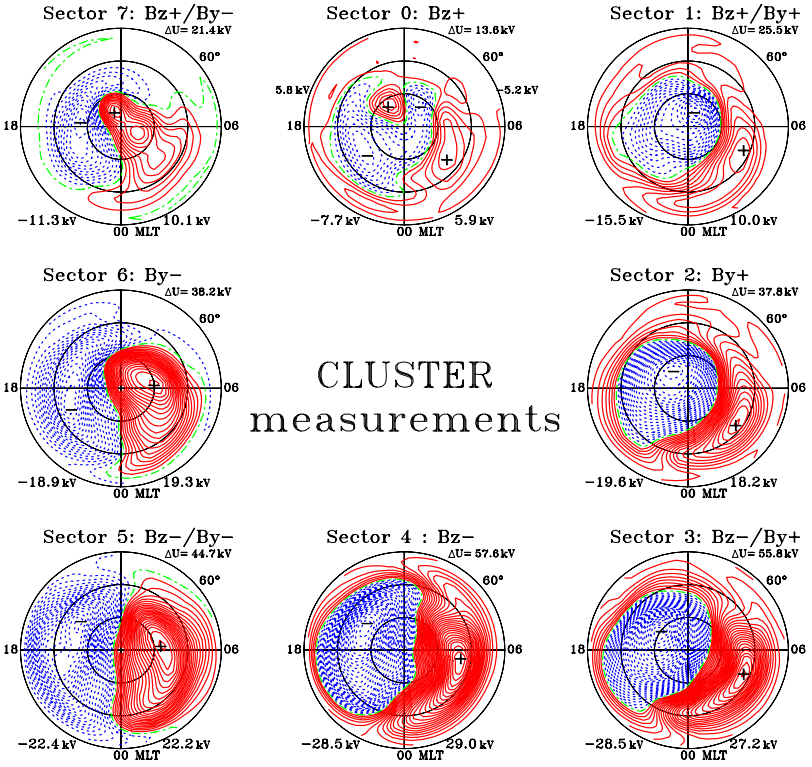

Fig. 1 Electric potentials obtained from CLUSTER observations for summer conditions at both northern and southern hemispheres. The potentials are shown as a function of MLAT/MLT for 8 sectors of IMF. The "+" and '-" signs indicate the positions the maximum and minimum potential values, respectively. The absolute maximum and minimum potentials are listed at the bottom with large character, and the total cross-polar drop at the upper right of each dial. The maximum and minimum potentials for daytime high-latitude vortices are listed additionally at the upper part of the Sector 0 (*Bz > 0*) dial. Positive potentials are marked by solid red lines, negative ones are marked by blue dotted lines. The potential lines are drawn at fixed potential values with a 1 kV spacing.

4) with an increasing IMF *By* component, the relative areas occupied by the positive and negative potential cells change with respect to each other, i.e., the area with negative (positive) potential increases for increasing IMF By^+ (By^-) values, which is equivalent to an overlayed circular convection cell with negative (positive) potential, over the pre-existing two-cell background pattern.

The large-scale convection high-latitude potential pattern could be represented by a relation like: $U = U_0 + Uy^{\pm} \times (\pm By) + Uz^{\pm} \times (\pm Bz)$, where U_0 represents a term which is independent on IMF, $Uy^{\pm}$ and $Uz^{\pm}$ describe the linear dependences on the IMF *By* and *Bz* components. Such a presentation of the potential patterns dependences on IMF has been used previously by *Feldstein and Levitin* [1986] for IZMEM model.

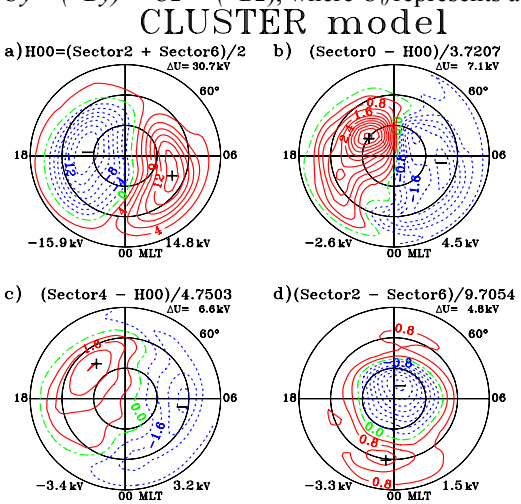

Fig. 2. Basic high-latitude convection patterns (BCPs) for summer conditions derived from EDU/CLUSTER observations sorted for different IMF orientation as shown in Fig. 1. The "H_{00}" background potential for vanishing *By* and *Bz* components (a) is derived as the sum of sectors 2 and 6 of Fig.1, while the IMF *By* dependence (d) is derived from their difference. The dependence on variations of the IMF *Bz* is shown separately for IMF Bz^+ (b) and IMF Bz^-(c) as derived from differences of sectors 0 and 4, respectively, to the "H_{00}" pattern.

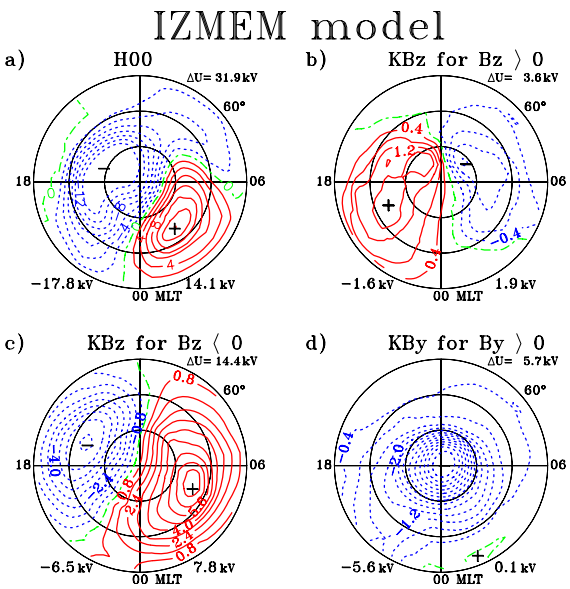

Fig.3. Basic high-latitude convection patterns (BCPs) as shown in Fig.2, but for the IZMEM model for summer solstice conditions in the Northern Hemisphere.

Fig. 2. shows four BCPs: U_0 (Fig2.a), Uy^+ (Fig2.d), Uz^+ (Fig2.b), Uz^- (Fig2.c). They are derived from summations of various sector's potential pattern that are shown in Fig. 1 (see the expressions at the top of each dial). The BCPs represent characteristic convection patterns for specific IMF conditions and the linear character of this representation allows to calculate convection pattern for any IMF conditions within reasonable ranges of applicability.

Corresponding BCPs representations for the IZMEM model (Northern hemisphere summer conditions) are shown in Fig. 3. The comparison with the EDI CLUSTER results in Fig. 2 shows a good correspondence for all four BCPs.

Fig. 4 presents six potential patterns for purely northward IMF with different values of the *Bz* component, which varies in steps of 1 nT from $Bz = 0$ nT to $Bz = 5$ nT. A two-cell pattern with antisunward convection prevails for the interval 0 nT $\leq Bz <$ 2 nT. Beginning with Bz = 2 nT, a second pair of convection cells with sunward drift between them appears on the dayside at high latitudes $> 80^o$, which is fully developed for Bz = 3 nT. The larger convection cells at lower latitudes with antisunward drift between them still prevail in strength. For Bz = 5 nT the high-latitude sunward convection cell pair dominates over the antisunward cells at lower latitudes. The BCP modelling of the EDI/CLUSTER data therefore confirm the patterns for $Bz \sim 4 \div 5$ nT magnitudes in Fig. 7 of *Förster et al*. [2008]. The addition of an IMF *By* convection to the U_0 + IMF Bz^+ system will result in a three-cell system.

Conclusions

The comparison of BCP representations obtained with EDI/CLUSTER and the corresponding patterns of the IZMEM model shows a good agreement of their characteristics. Two completely different data set and methods – the spatially distributed satellite measurements and the ground-based magnetometer data – confirm therefore the principal result, that the IMF dependence of the high-latitude plasma convection can be described as superposition of a background convection and linear variations with the IMF *By* and *Bz* components. This is valid for quasi-static conditions and moderate IMF variations; extreme parameter conditions have to be considered separately.

Acknowledgments. This study is supported by the Deutsche Forschungsgemeinschaft (DFG), the Norwegian Research Council, and the RFBR grants 08-05-00896, 07-05-13524.

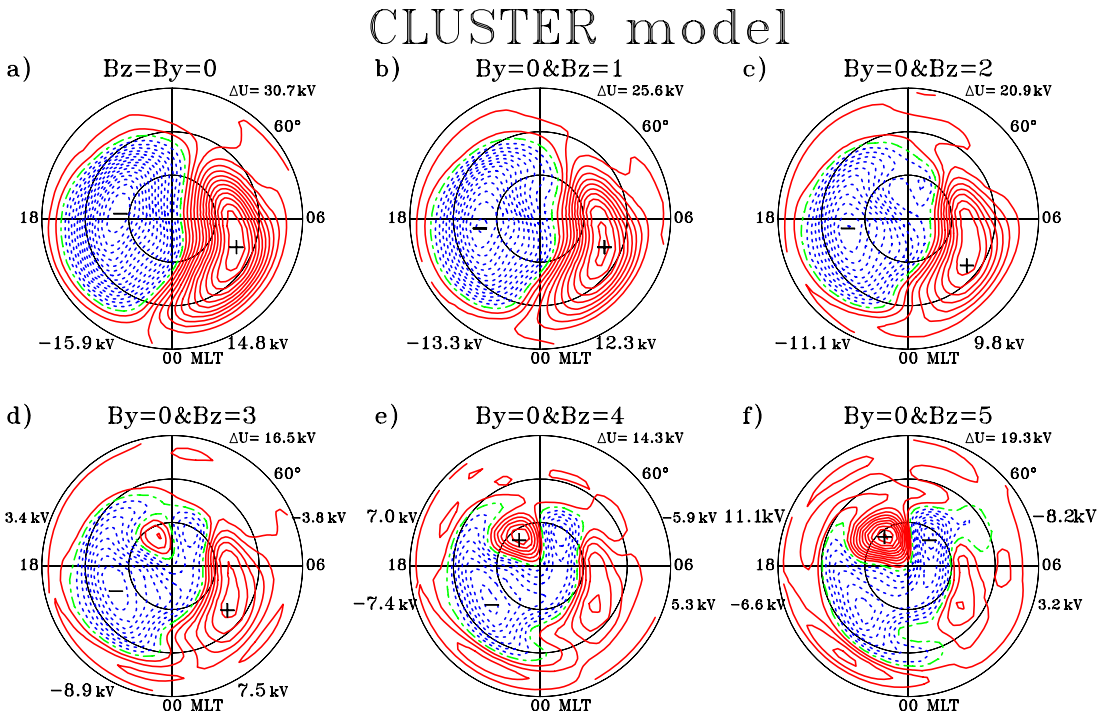

Fig. 4. CLUSTER model results for purely northward IMF, deduced from Fig.2. The values of the *Bz* components vary in step of 1 nT from *Bz* = 0 nT to *Bz* = 5 nT. The "+" and '-" signs indicate the positions of the absolute maximum and minimum potential values, respectively. The absolute maximum and minimum potentials are listed with large characters, and the total cross-polar drop at the upper right of each dial. The maximum and minimum potentials for additional daytime high-latitude vortices are listed at the upper part of the d)-dial; for additional vortices of night-early-morning sector at the right part of e)-dial; and for additional night-time vortices at the bottom part of f)-dial. Positive potentials are marked by solid red lines, negative ones are marked by blue dotted lines. The potential lines are drawn at fixed potential values with a 1 kV spacing.

References

1. Dremukhina L.A., Levitin A.E., Papitashvili V.O. Analytical representation of IZMEM model for near-real time prediction of electromagnetic weather, *J. Atmosph. Solar Terr. Phys*., 60, 1517, 1998.
2. Feldstein, Y.I., and Levitin, A.E., Solar wind control of electric fields and currents in the ionosphere, *J. Geomag. Geoelectr.*, 38, 1143, 1986.
3. Förster M., Paschmann G., Haaland S.E. et al. High-latitude plasma convection from CLUSTER EDI: Variances and solar wind correlations, *Ann. Geophys*., 25, 1691, 2007.
4. Förster M., Haaland S.E., Paschmann G. et al. High-latitude plasma convection during northward IMF as derived from in-situ magnetospheric CLUSTER EDI measurements, *Ann. Geophys*., 26, 2685, 2008.
5. Friis-Christensen E., Kamide Y., Richmond A.D., and Matsushita S. Interplanetary magnetic field control of high-latitude electric fields and currents determined from Greenland magnetometer data, *J. Geophys. Res*., 90, 1325, 1985.
6. Haaland S.E., Paschmann G., Förster M., et al. High-latitude plasma convection from CLUSTER EDI measurements: method and IMF-dependence, *Ann. Geophys*., 25, 239, 2007.
7. Haines G.V. Spherical cap harmonic analysis, *J. Geophys. Res*., B3, 90, 2583, 1985.
8. Heppner J.P. Empirical models of high-latitude electric fields, *J. Geophys. Res*., 82, 1115, 1977.
9 .Heppner J.P. and Maynard N.C. Empirical high-latitude electric field models, *J. Geophys. Res*., 92, 4467, 1987.
10. Papitashvili V.O. and Rich F.J. High – latitude ionospheric convection models derived from Defense Meteorological Satellite Program ion drift observations and parametrized by the interplanetary magnetic field strength and direction, *J. Geophys. Res*., 107, A8, 1198, 10.1029/2001JA000264, 2002.
11. Rich F.J. and Hairston M. Large-scale convection patterns observed by DMSP, *J. Geophys. Res*., 99, 3827,1994.
12. Ruohoniemi J.M. and Greenwald R.A. Dependencies of high-latitude plasma convection: Consideration of interplanetary magnetic field, seasonal and universal time factors in statistical patterns, *J. Geophys. Res*., 110, 9204, doi:1029/2004JA010815, 2005.
13. Tsyganenko N.A. A model of the near magnetosphere with a dawn-dusk asymmetry. 2. Parameterization and fitting of observations., *J. Geophys. Res*., 107, , doi: 10. 1029/2001JA000220, 2002.
14. Weimer D. Models of high-latitude electric potentials derived with a least error fit of spherical harmonic coefficients, *J. Geophys. Res*., 100, 19595, 1995.
15. Weimer D. Improved ionospheric electrodynamic models and application to calculating Joule heating rates, *J. Geophys. Res*., 110, A05306, doi: 10.1029/2004J010884, 2005.